

Nuclear Resonance Properties of $\text{YBa}_2\text{Cu}_3\text{O}_{6+x}$ Superconductors

R. E. WALSTEDT AND W. W. WARREN, JR.

Nuclear magnetic resonance (NMR) and nuclear quadrupole resonance (NQR) results for copper-63, oxygen-17, and yttrium-89 nuclei in the superconducting composition range of $\text{YBa}_2\text{Cu}_3\text{O}_{6+x}$ ($0.4 \leq x \leq 1.0$) are reviewed and interpreted. Copper NMR shift and susceptibility data, combined with a simple ionic model of local magnetic properties, yield a comprehensive analysis of the normal-state anisotropic susceptibility components and full characterization of the copper spin and orbital hyperfine couplings. Data on the spin-lattice relaxation time of these three nuclear species serve to characterize the highly correlated fermion dynamics in this system. Relaxation data from $\text{YBa}_2\text{Cu}_3\text{O}_7$ (superconducting transition temperature $T_c = 90$ K) and oxygen-deficient samples of this material ($T_c \sim 60$ K) have been analyzed in terms of mean-field models incorporating short-range antiferromagnetic order, giving a quantitative account of (planar) relaxation for these three nuclei in terms of a single dynamical susceptibility.

SINCE THEIR DISCOVERY IN 1986 (1), THE HIGH-TRANSITION temperature (T_c) superconducting copper oxides have presented a continuing challenge to solid-state physicists, chemists, and materials scientists. In the arena of basic scientific understanding, the key issue remains identification of the underlying mechanism responsible for the superconducting properties of these materials. Because the $3d$ shell is incomplete, there is the possibility that magnetism plays an important role in the superconductivity of copper oxides. With a formal valence slightly in excess of 2, the Cu configuration is approximately $3d^9$ so that each Cu atom carries an electron spin.

The importance of magnetism is further suggested by the existence of insulating, antiferromagnetic phases at compositions close to those of some of the superconductors. The superconducting phases are obtained from the antiferromagnetic phases by doping, that is, by changes of composition that increase the formal valence of Cu and introduce additional charge carriers (holes). These additional holes are not, however, created by removing more electrons from these Cu- $3d$ states. Rather, the holes take on primarily O- $2p$ character (2). Thus the Cu configuration remains close to $3d^9$, even though the formal valence would suggest considerable $3d^8$ character.

As a result of recent theoretical advances (3), the magnetic properties of the insulating, antiferromagnetic phases are quite well understood. Clarification of the role (if any) of magnetism in the

superconducting phases, that is, whether spin interactions produce superconductivity or compete with it (4), depends ultimately on a detailed understanding of the interactions between Cu- $3d$ holes and O- $2p$ holes at carrier concentrations high enough to permit superconductivity. It is clear that the Cu- $3d$ holes in the doped cuprates are itinerant, because their spins pair off and spin paramagnetism disappears at low temperatures. Nevertheless, depending on the detailed interplay between electron correlation and covalency, it is possible, in principle, for carriers to occupy different bands of electronic states having distinct dynamical characteristics. A number of workers have considered the possibility of multiple-band behavior (5, 6). In this article we present, in contrast, a viewpoint from which the microscopic magnetic properties can be understood in terms of carriers residing in a single band.

The nuclear resonance techniques, nuclear magnetic resonance (NMR) and nuclear quadrupole resonance (NQR), have emerged as key experimental probes in the effort to characterize the microscopic magnetic character of the high- T_c copper oxides. The power of these methods is derived largely from their highly local nature, which permits not only study of distinct chemical species in the compound but also selective measurements of different crystallographic sites for a given elemental constituent. The magnetic hyperfine interactions with unpaired valence electrons dominate the nuclear resonance characteristics, putting the nuclear spins "in touch with" microscopic electronic properties. Thus, for example, shifts of the NMR frequency or field are determined by various contributions to the static, uniform paramagnetism, whereas nuclear relaxation is governed by the fluctuation properties of the local spin hyperfine fields. Relaxation studies are particularly informative because the local electron spin dynamics are strongly influenced by the effects of correlation and itinerant behavior.

A large number of superconducting oxides are now known. Their structural chemistry was recently reviewed by Cava (7). Although many structural variations are possible, all these systems have in common the presence of two-dimensional CuO_2 planes, which most workers believe to be the site of the superconductivity. Many of these materials have now been investigated by NMR and NQR, but the most complete data, including results for $^{63,65}\text{Cu}$, ^{17}O , and ^{89}Y , are available for the "1-2-3" system $\text{YBa}_2\text{Cu}_3\text{O}_{6+x}$ (8-19). The fully ordered structure of the highest T_c phase ($\text{YBa}_2\text{Cu}_3\text{O}_{7.0}$, $T_c = 90$ K) exhibits narrow NMR and NQR lines unlike those of systems such as $(\text{La}_{1-x}\text{Sr}_x)_2\text{CuO}_4$ with cation disorder. Further, the interplay between Cu magnetism and carrier concentration in $\text{YBa}_2\text{Cu}_3\text{O}_{6+x}$ is easily manipulated by control of the O content. Because the associated O vacancies are located away from the CuO_2 planes, in the so-called Cu-O chain layer, perturbations of the local environments in the planes are minimal. The $\text{YBa}_2\text{Cu}_3\text{O}_{6+x}$ system is insulating and antiferromagnetic over the composition range $0 \leq x \leq 0.4$ and is metallic and superconducting for $0.4 \leq x \leq 1.0$

The authors are at AT&T Bell Laboratories, Murray Hill, NJ 07974.

(20). For samples of this material prepared at relatively low temperatures, T_c is roughly independent of x over the range $0.5 \leq x \leq 0.7$ with a value $T_c \sim 60$ K.

It is the aim of this article to summarize the progress achieved as a result of NMR and NQR studies during the past 3 years, emphasizing the interpretation of results obtained for the CuO_2 planes in $\text{YBa}_2\text{Cu}_3\text{O}_{6+x}$. We first consider the static NMR properties of the stoichiometric 90 K phase $\text{YBa}_2\text{Cu}_3\text{O}_{7.0}$. We then turn to the relaxation behavior of this phase, both above and below T_c . Finally, we examine the highly contrasting, but apparently closely related behavior of the O-deficient phase with $T_c \sim 60$ K.

NMR Shifts and the Magnetic Susceptibility: An Ionic Model

One of the most important recent developments is the emergence of a simple model, based on well-established concepts, that yields at least a semiquantitative analysis of the normal-state magnetic and hyperfine behavior of $\text{YBa}_2\text{Cu}_3\text{O}_{6+x}$. In general, a paramagnetic metal is characterized by a spin susceptibility (21) $\chi_s(\mathbf{q}, \omega) = \chi'_s(\mathbf{q}, \omega) + i\chi''_s(\mathbf{q}, \omega)$, which is a function of wave vector \mathbf{q} and frequency ω (22). We consider first the static, uniform susceptibility $\chi'_s(0, 0)$, which, when added to Van Vleck orbital (23) and core diamagnetic terms, determines the total, experimentally observed susceptibility at $T > T_c$:

$$\chi_{\text{expt}, \nu} = \chi'_{s, \nu}(0, 0) + \chi_{\text{orb}, \nu} + \chi_{\text{dia}} \quad (1)$$

where $\nu = a, b, c$ specifies the crystal axis along which the magnetic field is directed.

Extensive experience with d -band metals and compounds dating back to the 1960s has shown that NMR shift data may often be used to decompose the susceptibility into its component parts, yielding in addition values for the hyperfine couplings (24). To apply this analysis (25) to $\text{YBa}_2\text{Cu}_3\text{O}_{7.0}$, it is useful first to break down $\chi_{\text{orb}, \nu}$ and $\chi'_{s, \nu}(0, 0)$ into contributions that reside primarily (26) on the Cu(1) chain and Cu(2) plane sites (see Fig. 1). Thus,

$$\chi_{\text{orb}, \nu} = \chi_{1\nu}^{\text{orb}} + 2\chi_{2\nu}^{\text{orb}} \text{ and } \chi'_{s, \nu}(0, 0) = \chi_{1\nu}^s + 2\chi_{2\nu}^s \quad (2)$$

The NMR shifts K (27) of the Cu nuclei have spin and orbital (28) components $K_{1,2\nu} = K_{1,2\nu}^s + K_{1,2\nu}^{\text{orb}}$, which are proportional to the susceptibilities in Eq. 2, that is,

$$K_{1,2\nu}^{\text{orb}} = \alpha_{\text{orb}} \chi_{1,2\nu}^{\text{orb}} \text{ and } K_{1,2\nu}^s = \alpha_{1,2\nu}^s \chi_{1,2\nu}^s \quad (3)$$

where $\alpha_{1,2\nu}^s$ and α_{orb} are the spin and orbital shift coefficients, respectively (29).

Key experiments for the success of the K - χ analysis include the measurement (16) of the anisotropy of χ_{expt} , that is, $\chi_{\text{expt}, ab}$ and $\chi_{\text{expt}, c}$, and the use of single-crystal and oriented powder specimens to obtain narrow NMR spin echo lines and accurate shift data (6, 14–16), even in the presence of strong electric quadrupole interactions. In Fig. 2 we plot c -axis ($\nu = c$) and in-plane ($\nu = ab$) NMR shifts versus T for the planar Cu(2) sites in both the 90 K and 60 K phases of $\text{YBa}_2\text{Cu}_3\text{O}_{6+x}$. The results for K_{2ab} in the 90 K phase illustrate the loss of the spin-paramagnetic shift for $T < T_c$ in spin-paired superconductors (30). Below T_c , K_{2ab} declines sharply, losing about half of its normal-state value as $T \rightarrow 0$. The asymptotic ($T \rightarrow 0$) shift values are interpreted as the orbital components (16), which are assumed to be independent of temperature. The change $K_{2ab}(T) - K_{2ab}(T \rightarrow 0)$ is the spin component. The change of K_{2c} below T_c is anomalously small. Shift components obtained in this fashion (6, 16) and recent susceptibility data (31) are summarized in Table 1.

Magnetic and hyperfine data for the 90 K phase $\text{YBa}_2\text{Cu}_3\text{O}_{7.0}$

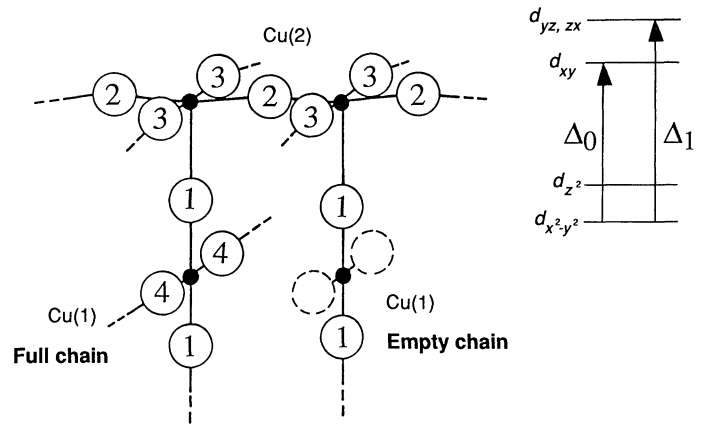


Fig. 1. Section of the $\text{YBa}_2\text{Cu}_3\text{O}_{6+x}$ lattice showing neighboring Cu(1) and Cu(2) sites with their O ligands, which are numbered. For material with $x < 1$, the O(4) sites are partially empty as shown. Relevant crystal field energies for the Cu(2) sites, in hole notation, are shown at the right, where $xyz \equiv abc$. The Y^{+3} sites lie above the Cu(2) plane and are equidistant from four Cu(2) sites in the plane shown.

have been analyzed by Mila and Rice (25), using an ionic (Cu^{2+}) model for which the detailed properties have been worked out in spin Hamiltonian theory (32). The validity of such a model, more typically used for ions with a fully localized, permanent magnetic moment, might be questioned in view of the clearly itinerant character of the Cu-3d holes. The itinerant character of the d -holes is evidenced by the freeze-out of spin paramagnetism and, as we shall discuss shortly, nuclear spin-lattice relaxation at $T \ll T_c$. However, the Cu-3d bands in $\text{YBa}_2\text{Cu}_3\text{O}_{7.0}$ are quite narrow (33). In a tight-binding model of these bands, many simple attributes such as the electronic g -tensor, the hyperfine tensor, and the Van Vleck orbital paramagnetism are expected to carry over from the localized picture with only minor modifications.

We can convey the essence of the ionic picture by considering the planar Cu sites, for which the ground state is a nearly pure $d_{x^2-y^2}$ orbital with excited states d_{xy} and d_{yz}, d_{zx} at energies Δ_0 and Δ_1 , respectively (Fig. 1, inset) (32). These excited states account for the orbital susceptibility ($\chi_{\text{orb}, ab}$, $\chi_{\text{orb}, c}$) (34). They also give rise, through the spin-orbit Hamiltonian term $\lambda \mathbf{L} \cdot \mathbf{S}$ (where λ is coupling strength, \mathbf{L} is angular momentum, and \mathbf{S} is spin), to an electronic g -shift (35) and modified spin hyperfine constants (36). The hyperfine Hamiltonian for Cu(2) site nuclear spin \mathbf{I}_i takes the form

$$H_{\text{hf}} = \sum_{\alpha} A_{\alpha} I_{i\alpha} S_{i\alpha} + \mathbf{B} \mathbf{I}_i \cdot \sum_{j(mn)} \mathbf{S}_j \quad (4)$$

where the second term describes a transferred hyperfine field from nearest neighbor Cu(2) spins \mathbf{S}_j ($S = 1/2$). The B term is necessary to account for the observed anisotropy of the nuclear spin-lattice relaxation time T_1 of the Cu(2) nuclei (37). T_1 measurements reveal that the c -axis hyperfine fluctuations are predominant, in apparent conflict with the result $K_{2c}^s \ll K_{2ab}^s$ (Table 1). The B terms resolve this difficulty, because the \mathbf{S}_j fluctuate somewhat independently, even though the shift coefficient $\alpha_{2c}^s \propto A_c + 4B \sim 0$. With the more recent data (Table 1), it is possible to take account of g -shift anisotropy (35) and to determine the parameters $\langle r^{-3} \rangle$, Δ_0 , Δ_1 , and B from a self-consistent solution of Eqs. 1 through 4 (38) by use of the ancillary relations from the ionic model (34–36). The results are given in Table 2.

The values given in Table 2 differ in only minor ways from the results of earlier analyses (25) and are completely consistent with expectations derived from studies of other 3d systems. The value of $\langle r^{-3} \rangle$ is smaller than that of an isolated Cu^{2+} ion [6.3 atomic units (au)] (32), more in line with values appropriate to the 3d metals

Table 1. NMR shift components for the Cu(1) and Cu(2) sites in $\text{YBa}_2\text{Cu}_3\text{O}_{7.0}$ derived from data such as that shown in Fig. 2 (6), and anisotropic susceptibility data at $T = 100$ K from (31). Shifts are in percent; susceptibilities are in 10^{-6} emu/mol formula unit.

	$K_{1\nu}^{\text{orb}}$	$K_{1\nu}^{\text{s}}$	$K_{2\nu}^{\text{orb}}$	$K_{2\nu}^{\text{s}}$	χ_{ν}^{expt}
$H \parallel c$	0.25	0.33	1.28	-0.01	392
a	1.08	0.25			
$H \perp c$			0.28	0.30	240
b	0.27	0.29			

Table 2. Susceptibility, hyperfine, and ionic parameters for Cu(2) derived from the analysis based on Eqs. 1 through 4. See text and (34-36) for definitions. The χ 's are given in 10^{-6} emu/mol, A_{ν} and B are in kilogauss per Bohr magneton, the Δ values are in electron volts, and $\langle r^{-3} \rangle$ is in atomic units.

ν	g_{ν}	$\chi_{2\nu}^{\text{s}}$	$\chi_{2\nu}^{\text{orb}}$	A_{ν}	B	$\langle r^{-3} \rangle$	Δ_0	Δ_1
c	2.36	111	106.4	-188.4	44.6	5.37	1.97	2.25
ab	2.08	104	23.3	-11.2				

(39). The crystal field splittings ($\Delta_{0,1}$) are in good agreement with theoretical estimates (40). As expected, the g -factor anisotropy is comparable to, but somewhat larger than, that of cubic Cu metal (41). The anisotropy of χ_2^{s} is not as great as that of g , probably reflecting a lower or possibly reverse anisotropy for the Cu(1) site component, which is not distinguished from that of Cu(2) in this calculation (38). The latter assumption and the unknown admixture of d_{z^2} orbital (Fig. 1) into the ground state are the major sources of uncertainty for the parameter values given in Table 2. Finally, the magnitude of the spin susceptibility, when compared with predictions based on the band theory densities of states (33), indicates that $\chi_2^{\text{s}}(0,0)$ is only weakly enhanced (\sim two to three times) relative to the noninteracting limit. This is of central importance in relation to the spin dynamics.

Spin Dynamics in $\text{YBa}_2\text{Cu}_3\text{O}_{7.0}$

Given the success of the spin-paramagnetic description of the static magnetic properties of $\text{YBa}_2\text{Cu}_3\text{O}_{7.0}$, there is good reason to assume that nuclear relaxation in the normal state is also driven by spin hyperfine interactions. These interactions couple the nuclei to the dissipative term $\chi_2^{\text{s}}(\mathbf{q}, \omega)$ of the generalized susceptibility. It is important to recognize, however, that nuclei in d -band metals can also be relaxed very effectively by orbital currents (42). For example, it was recently proposed that charge excitations dominate the relaxation process through the orbital mechanism (43). In the particular case of $\text{YBa}_2\text{Cu}_3\text{O}_{6+x}$, the $3d$ holes at the Cu(2) sites have $d_{x^2-y^2}$ symmetry (with possibly a small admixture of d_{z^2} (33), for which the relaxation matrix elements vanish. In this discussion we shall assume the orbital relaxation process to be negligible.

Well-established theory (44) relates the nuclear relaxation rate $(T_1)^{-1}$ to spin fluctuations via the spin hyperfine couplings:

$$(T_1 T)_{\text{Cu}(2)}^{-1} = \frac{k_B}{\gamma_2^2 \hbar^4} \sum_{\mathbf{q}} \{ [A_x + 2Bf_2(\mathbf{q})]^2 + [A_y + 2Bf_2(\mathbf{q})]^2 \} [\chi_2^{\text{s}}(\mathbf{q}, \omega)/\omega]_{\omega \rightarrow 0} \quad (5)$$

where k_B is the Boltzmann constant, \hbar is Planck's constant, and $A_{x,y}$ are the on-site hyperfine field components perpendicular to the axis of quantization (magnetic field direction for NMR or electric field

Fig. 2. The closed symbols show the variation of the Cu(2) NMR shift with temperature for $\text{YBa}_2\text{Cu}_3\text{O}_{7.0}$ (6) with the field parallel (K_{2c} , squares) and perpendicular (K_{2ab} , circles) to the c -axis. The solid line is a guide to the eye, showing the very nearly constant shift K_{2ab} in the normal state [see (15)]. The open symbols show corresponding data (60) for $\text{YBa}_2\text{Cu}_3\text{O}_{6.64}$. The latter data are discussed in the subsection on the 60 K phase. Typical error bars are shown.

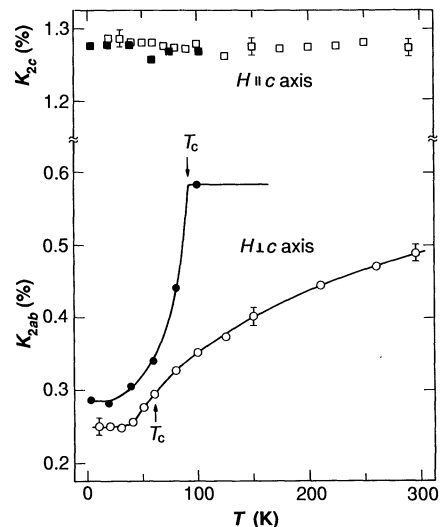
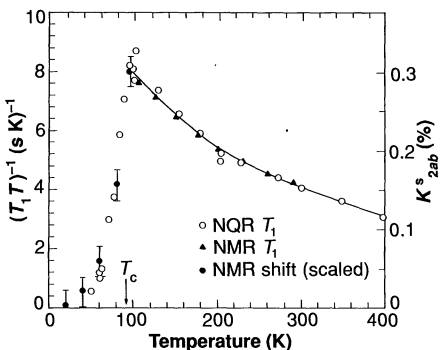


Fig. 3. Data for the spin-lattice relaxation time T_1 of $\text{YBa}_2\text{Cu}_3\text{O}_7$ are plotted as $(T_1 T)^{-1}$ versus T , for temperatures both above and below T_c . Data taken at both zero field [NQR (10)] and in a field $H \sim 7.5$ T [NMR (37)] agree within the experimental errors, verifying that T_1 is field-independent. Also plotted are values of the Cu(2) spin shift K_{2ab}^{s} (27) (solid circles), scaled to coincide with the T_1 data at $T \sim 100$ K, showing that $(T_1 T K_{2ab}^{\text{s}})^{-1}$ is very nearly constant below T_c .



gradient tensor principal axis for NQR). Because the isotropic hyperfine field B couples nuclei to spin fluctuations on neighboring Cu(2) sites, it is necessary to include the geometric form factor $f_2(\mathbf{q})$ (45). The sum over q is taken over all q values so that spin correlations of quite short wavelength (comparable with interatomic dimensions) can make important contributions to spin-lattice relaxation.

The intensity of low-frequency spin fluctuations depends on two essential factors. One factor, proportional to $\chi_2^{\text{s}}(0,0)$, is related to the effective number of spins interacting with the nucleus. The second, a correlation time τ_c , characterizes the time scale of the fluctuations. For the familiar case of weakly correlated electrons in an ordinary metal, both factors are independent of temperature [$\tau_c = \hbar N(E_F)$, where $N(E_F)$ is the density of states at the Fermi energy] leading to the Korringa behavior (46), $T_1 T = \text{constant}$.

Nuclear relaxation data $(T_1 T)^{-1}$ can be obtained for individual crystalline sites with the use of either the appropriate NQR lines or NMR lines in oriented powders. Results for the Cu(2) sites in $\text{YBa}_2\text{Cu}_3\text{O}_{7.0}$ are shown as a function of temperature in Fig. 3. It is obvious that the Korringa behavior is not observed because $(T_1 T)^{-1}$ increases steadily with decreasing temperature down to T_c . Below T_c , $(T_1 T)^{-1}$ drops precipitously, as we discuss in more detail below. T_1 may be estimated from the values of the shifts $K_{2\nu}^{\text{s}}$ (Table 1), assuming noninteracting conduction electrons (46). This estimate shows that the measured Cu(2) relaxation rate is enhanced by roughly an order of magnitude near T_c (see Fig. 4 and discussion below). The electron spin dynamics are therefore strongly modified by electron-electron interactions. As noted earlier, the uniform ($\mathbf{q} =$

0) susceptibility is not greatly enhanced. It follows, then, from Eq. 5 that the relaxation enhancement arises from some range of non-zero q values. The simplest interpretation of this enhancement is in terms of spin fluctuations, because these would be expected to introduce a peak in $[\chi_s''(\mathbf{q},\omega)/\omega]_{\omega \rightarrow 0}$ near the antiferromagnetic wave vector \mathbf{q}_{AF} .

Nuclear relaxation rates for the Y and planar O(2,3) nuclei provide additional insight, because their relaxation behavior is strikingly different from that of Cu(2). Korringa temperature dependence ($T_1 T = \text{constant}$) is observed for Y and O(2,3), and there is only weak enhancement relative to the noninteracting limit (18, 47). How can this be explained? An obvious possibility is a two-band situation in which Y and O(2,3) nuclei, on the one hand, and Cu(2), on the other, couple to different sets of spins with distinct dynamics. But it is not easy to understand how such dramatically different spin dynamics could survive in the presence of the strong Cu-3d-O-2p hybridization and exchange interactions between neighboring sites. Moreover, as we discuss below, the spin susceptibilities of all planar sites are suppressed with a common temperature dependence below the onset of superconductivity.

These difficulties are resolved in a natural way if we invoke a single-band description and make the reasonable assumption that the antiferromagnetic spin fluctuations are commensurate with the lattice (or nearly so). If we follow arguments well known from studies of ligand relaxation in magnetic compounds (47) and introduced to the present problem by Hammel *et al.* (48), it is easy to see that the hyperfine field vanishes at an O site equidistant between two oppositely aligned Cu spins (45). More precisely, the crystalline symmetry introduces form factors (45, 49) in the expressions analogous to Eq. 5 for O(2,3) and Y, which vanish at the commensurate antiferromagnetic wave vector $\mathbf{q}_{AF} = (\pi/a, \pi/b)$, where the Cu(2) form factor $f_2(\mathbf{q})$ reaches a maximum. The form factors thus filter the influence of $[\chi_s''(\mathbf{q},\omega)/\omega]_{\omega \rightarrow 0}$ such that only the Cu(2) rate is highly sensitive to the high- q antiferromagnetic fluctuations, whereas the Y and O(2,3) relaxations are determined by $[\chi_s''(\mathbf{q},\omega)/\omega]_{\omega \rightarrow 0}$ at low q values where the enhancement is small.

Up to the present time, no detailed theory of spin dynamics in the doped cuprates has been put forward. However, mean-field theories by Bulut *et al.* (50) and by Millis *et al.* (51) and a closely related phenomenological model by Varma *et al.* (52) give encouraging preliminary results. The mean-field models give a low-frequency imaginary susceptibility component of the form

$$[\chi_s''(\mathbf{q},\omega)/\omega]_{\omega \rightarrow 0} \propto \chi_s'(0,0)g(\mathbf{q}) \quad (6)$$

in which the dynamics are modeled by $g(\mathbf{q})$ (50, 51). In the model of Millis *et al.* (51), for example, $g(\mathbf{q})$ is enhanced at $\mathbf{q} = (\pi/a, \pi/b)$ by a peak whose width varies inversely as the square of the antiferromagnetic correlation length ξ . With a temperature-dependent ξ , these investigators are able to simulate the relaxation enhancements and temperature dependences for Cu(2), O(2,3), and Y nuclei coupling to the same spin fluctuations. The model also accounts correctly for the observed anisotropy (37) of the Cu(2) relaxation. The antiferromagnetic correlation lengths, although admittedly model-dependent, are quite short: $\xi \sim 2a$ to $3a$ at T_c , where a is the lattice constant. However, even these correlation lengths correspond to very strong enhancement of the high- q susceptibility, which must be justified by a first-principles theory of the spin dynamics in these systems.

The Superconducting State

In the conventional Bardeen-Cooper-Schrieffer (BCS) theory of superconductivity and, indeed, in most models proposed for the high- T_c materials, the electron spin degrees of freedom are sup-

pressed in the superconducting ground state. The spin susceptibility then vanishes, as do the spin hyperfine contributions to nuclear magnetic relaxation and the NMR shift (30). At non-zero temperatures below T_c , NMR shifts and nuclear relaxation are produced by thermal excitations of the superconductor (quasi-particles). The functional form of the temperature dependence of $(T_1)^{-1}$ in this range depends on details of the quasi-particle excitation spectrum. For the most familiar case, namely, BCS "s-wave" superconductivity, an energy gap $\Delta(T)$ opens symmetrically at all points of the Fermi surface leading to a Hebel-Slichter "peak" (53) in $(T_1)^{-1}$ at $T \approx T_c$ and an exponential variation $(T_1)^{-1} \propto \exp(-\Delta/kT)$ when $T \ll T_c$.

As shown in Fig. 3, $(T_1 T)^{-1}$ for Cu(2) drops sharply with decreasing temperature below T_c with no hint of the expected Hebel-Slichter peak. Relaxation data for the Y (8) and planar O nuclei (48) show similar behavior. Model calculations in which this peak is absent owing to pair-breaking interactions have been put forward by Kuroda and Varma (54) and by Coffey (55). Moreover, exponential fits to the low-temperature T_1 data on the assumption of an "s-wave" energy gap yield gap values in the range $2\Delta \sim 8k_B T_c$ or possibly larger (8, 10, 11). It has been difficult to establish the detailed nature of the gap, however, because of the presence of extrinsic relaxation at low temperatures (56). Despite being weaker than the relaxation at T_c by some four orders of magnitude, the background relaxation prevents accurate measurement of the intrinsic temperature dependence of $(T_1)^{-1}$ at $T \ll T_c$.

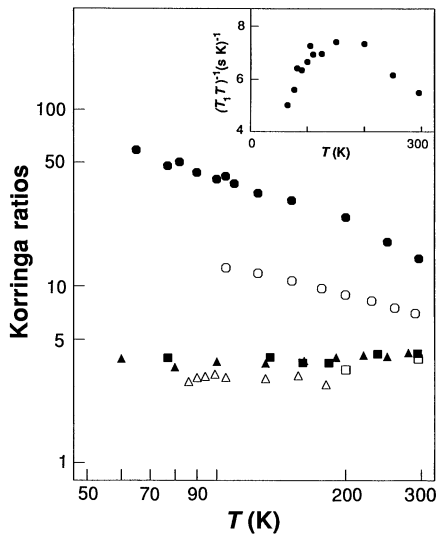
Below T_c , the O(2,3) relaxation rate is found (48) to be very nearly proportional to the Cu(2) rate down to at least $T \sim T_c/5$. Also, $(T_1 T)^{-1}$ for both nuclei are, within experimental error, proportional to the spin part of the NMR shift K_{ab}^s and, by implication, to the spin susceptibility (Fig. 3). These observations show that the susceptibilities probed by the resonance experiments, $\chi_s'(0,0)$ and $[\chi_s''(\mathbf{q},\omega)/\omega]_{\omega \rightarrow 0}$, are suppressed in the superconducting state with the same temperature dependence at all q values. There is no change in the relative enhancement at various q values because this would affect the ratio of the Cu(2) and O(2,3) relaxation rates. In the spirit of Eq. 6, the temperature dependence at $T < T_c$ arises from the effective density of spin excitations $[\chi_s'(0,0)]$, while the dynamics of those excitations remain fixed and characteristic of the normal state at T_c .

Spin Paramagnetism and Dynamics in the $T_c = 60$ K Phase

Removal of 30 to 50% of the O(4) chain oxygens (see Fig. 1) from $\text{YBa}_2\text{Cu}_3\text{O}_{7.0}$ leads to a phase with composition-independent T_c values (~ 60 K) extending nearly to the superconducting-antiferromagnetic phase boundary [see figure 3a in (20)]. X-ray absorption (57) and NMR studies (58) of this phase demonstrate that the O vacancies order to form "full" (that is, no vacancies) and "empty" chains (Fig. 1). NQR spectra (59) show further that there is no desegregation on a macroscopic scale. The full and empty chains provide a modulated environment for the neighboring planar sites, which gives rise to resolved structure in the NQR spectrum (59) but only slightly broadens the distribution of NMR shifts (60).

Results for the Cu(2) shifts from a sample of $\text{YBa}_2\text{Cu}_3\text{O}_{6.64}$ are given in Fig. 2. The c -axis shift K_{2c} is essentially indistinguishable from that of the 90 K phase, which tells us that the orbital shift K_{2c}^{orb} is invariant and that the near cancellation of hyperfine coefficients giving $K_{2c}^s \sim 0$ (Table 1) continues to hold. Thus, the basic ionic and hyperfine properties of the Cu(2) site are invariant under the removal of O and concomitant reduction in carrier density within the metallic phase. In contrast, the spin paramagnetism as reflected

Fig. 4. Values of the modified Korringa ratio for $T_c = 60$ K material (solid symbols) are compared with values of the ordinary Korringa ratio for $T_c = 90$ K material (open symbols). See text for definitions. Data for the 60 K phase are Cu(2) [closed circles (60)], O(2,3) [closed triangles (61)], and Y [closed squares (18)]. Data for the 90 K phase are Cu(2) [open circles (37)], O(2,3) [open triangles, new data], and Y [open squares (17)]. The plot shows the growing antiferromagnetic fluctuations at the Cu(2) sites in both phases as T is lowered, which are not “seen” by the O(2,3) or Y sites. The inset shows the source relaxation data (59) for the 60 K Cu(2) (uppermost) curve.



in the transverse shift K_{2ab}^s (Fig. 3) becomes smaller in the 60 K phase and becomes strongly temperature-dependent, diminishing as $T \rightarrow T_c$ by a factor of ~ 5 relative to its value at 300 K. Furthermore, there is little or no change in the curve at T_c , in striking contrast with the 90 K phase result (Fig. 2). Similar behavior is observed for the Y (18) and O(2,3) (61) sites, again underscoring single-band behavior for the planes in this compound. The physical significance of this dramatic decline in the Pauli paramagnetism for the 60 K phase has yet to be established. Friedel (62) has suggested an explanation in terms of a pseudo-gap near the Fermi surface caused by the scattering of carriers by antiferromagnetic short-range correlations. Such pseudo-gap behavior is possibly a consequence of the spin bag model (63).

Suppression of $\chi_s(0,0)$ in the normal state also suggests an explanation for the peculiar temperature dependence of the relaxation for the Cu(2) sites in the 60 K phase, where $(T_1 T)^{-1}$ reaches a maximum just above $T = 100$ K and descends sharply as T approaches T_c (Fig. 4, inset) (59). To interpret this T_1 behavior we use the model form of Eq. 6 for $\chi''(\mathbf{q},\omega)$, which implies that by plotting the quantity $(T_1 T K_{2ab}^s)^{-1}$ we can separate the behavior of the antiferromagnetic fluctuations represented by $g(\mathbf{q})$ from that of $\chi_s'(0,0) \propto K_{2ab}^s$. In order to render this into a form independent of hyperfine properties, we multiply the ordinary Korringa ratio (46) $T_1(\text{Korr.})/T_{1c}$ by $[K_{2ab}^s/K_{2ab}^s(300 \text{ K})]$, where $(T_1(\text{Korr.})T)^{-1} = 4\pi k_B \gamma_n^2 K_{2ab}^s / (N_s \gamma_e^2 \hbar)$ (64). This yields a “modified Korringa ratio” (MKR), $[T_1(\text{Korr.})/T_{1c}](K_{2ab}^s/K_{2ab}^s(300 \text{ K}))$. The MKR reduces to the ordinary Korringa ratio for the 90 K phase, because the shifts are very nearly temperature-independent in that case. Figure 4 compares the MKR for Cu(2) (60), O(2,3) (61), and Y (18) in the 60 K samples (17, 37).

The antiferromagnetic fluctuations reflected by the Cu(2) results vary with temperature in the same way in both phases but are much stronger in the 60 K phase. Interpretation in terms of the mean-field model of Millis *et al.* (51) suggests that the correlation lengths are much longer ($5a$ to $6a$) in $\text{YBa}_2\text{Cu}_3\text{O}_{6.64}$ than in $\text{YBa}_2\text{Cu}_3\text{O}_{7.0}$. This trend is reasonable, because the 60 K phase is much closer to the antiferromagnetic phase boundary. The O(2,3) and Y sites exhibit a low background enhancement effect for both phases but are impervious to the antiferromagnetic fluctuations as noted in the previous section. A unified interpretation for spin dynamics in both phases is therefore achieved with Eq. 6.

Summary

As a result of the contributions of many research groups, we now have a fairly complete experimental picture of $\text{YBa}_2\text{Cu}_3\text{O}_{6+x}$ based on NMR and NQR. The experiments have established a set of microscopic electronic properties with which any successful theory must be consistent. Moreover, the results available for planar sites in related systems are similar in many respects to those of the planar Cu(2) sites in $\text{YBa}_2\text{Cu}_3\text{O}_{6+x}$. This similarity offers some reason to hope that the following conclusions drawn from this “fruit fly” system may be generalized to the whole class of cuprate superconductors.

Spin paramagnetism in the normal state. A simple ionic model of the static spin and orbital paramagnetism yields quantitative determinations of susceptibility components, crystal field splittings, hyperfine couplings, and NMR shift and relaxation anisotropy. Spin paramagnetism makes major contributions to NMR shifts and relaxation in the normal state.

Itinerant character of Cu-3d electrons. The NMR shifts and nuclear relaxation below T_c show that the Cu-3d spins participate fully in the superconducting ground state. Superconductivity cannot be the exclusive property of a band of itinerant O-2p holes.

Antiferromagnetic fluctuation dynamics. A scenario in which nuclear relaxation processes are dominated by spin fluctuation dynamics, and the latter represented by mean-field models incorporating antiferromagnetic short-range order within a single band, gives a quantitative account of the magnitude, anisotropy, and temperature dependence of T_1 values at all the planar sites in the metallic phases.

Suppression of antiferromagnetic fluctuations by doping. The antiferromagnetic correlation lengths are sharply reduced with increasing carrier concentration.

Weakly enhanced uniform spin susceptibility. The static, uniform spin susceptibility is only modestly enhanced relative to the noninteracting limit represented by band theory.

Temperature-independent spin dynamics of excited quasi-particles below T_c . The generalized susceptibility at low frequencies $\chi_s(\mathbf{q},\omega_0)$ is uniformly suppressed at all q values in the superconducting state. Thermally excited quasi-particles exhibit temperature-independent spin fluctuations characteristic of the normal metal at T_c .

Temperature-dependent suppression of the uniform susceptibility in the normal state of the lightly doped system. The spin susceptibility is sharply reduced as $T \rightarrow T_c$ in the normal state of the 60 K superconductor, due, perhaps, to a reduction of the density of states. At the same time, antiferromagnetic fluctuations are increasingly enhanced among those spins that contribute to the susceptibility.

REFERENCES AND NOTES

1. J. G. Bednorz and K. A. Müller, *Z. Phys. B* **64**, 189 (1986).
2. V. J. Emery, *Phys. Rev. Lett.* **58**, 2794 (1987); N. Nücker *et al.*, *Phys. Rev. B* **37**, 5158 (1988).
3. R. R. P. Singh, M. P. Gelfand, D. A. Huse, *Phys. Rev. Lett.* **61**, 2484 (1988); S. Chakravarty, B. I. Halperin, D. R. Nelson, *Phys. Rev. B* **39**, 2344 (1989).
4. P. Littlewood, C. M. Varma, E. Abrahams, *Phys. Rev. Lett.* **63**, 2602 (1989).
5. V. J. Emery and G. Reiter, *Phys. Rev. B* **38**, 11938 (1989); Y. Kitaoka *et al.*, *Physica C* **162–164**, 195 (1989); B. R. Trees and D. L. Cox, *Bull. Am. Phys. Soc.* **35**, 784 (1990).
6. S. Barrett *et al.*, *Phys. Rev. B* **41**, 6283 (1990).
7. R. J. Cava, *Science* **247**, 656 (1990).
8. J. T. Markert, T. W. Noh, S. E. Russek, R. M. Cotts, *Solid State Commun.* **63**, 847 (1987).
9. H. Lütgemeier and M. W. Pieper, *ibid.* **64**, 847 (1987).
10. W. W. Warren, Jr., R. E. Walstedt, G. F. Brenner, G. P. Espinosa, J. P. Remeika, *Phys. Rev. Lett.* **59**, 1860 (1987).
11. M. Mali *et al.*, *Phys. Lett. A* **124**, 112 (1987).
12. E. Lippmaa *et al.*, *Physica C* **153–155**, 95 (1988).
13. Y. Kitaoka, S. Hiramatsu, T. Kondo, K. Asayama, *J. Phys. Soc. Jpn.* **57**, 30 (1988).
14. T. Imai *et al.*, *ibid.*, p. 2280.
15. C. H. Pennington *et al.*, *Phys. Rev. B* **37**, 7944 (1988).
16. M. Takigawa, P. C. Hammel, R. Heffner, Z. Fisk, *ibid.* **39**, 7371 (1989).

17. G. Balakrishnan, R. Dupree, I. Farnan, D. McK. Paul, M. E. Smith, *J. Phys. C* **21**, 1847 (1988).
18. H. Alloul, T. Ohno, P. Mendels, *Phys. Rev. Lett.* **63**, 1700 (1989).
19. A. J. Vega, W. E. Garneth, E. M. McCarron, R. K. Bordia, *Phys. Rev. B* **39**, 2322 (1989).
20. R. J. Cava *et al.*, *Physica C* **156**, 523 (1988).
21. For the 3d metals the spin-orbit coupling mixes a small amount of orbital character into $\chi_s(\mathbf{q}, \omega)$.
22. For a discussion of dynamic susceptibilities, see R. M. White, in *Quantum Theory of Magnetism*, Springer Series in Solid-State Sciences, vol. 32, P. Fulde, Ed. (Springer-Verlag, New York, 1983), chap. 1.
23. J. H. Van Vleck, *Electric and Magnetic Susceptibilities* (Oxford Univ. Press, Oxford, 1932).
24. A. M. Clogston, V. Jaccarino, Y. Yafet, *Phys. Rev. A* **134**, 650 (1964).
25. F. Mila and T. M. Rice, *Physica C* **157**, 561 (1989).
26. The orbital susceptibility arises almost exclusively from the Cu-3d electrons. The spin polarization is understood to reside mainly on the Cu sites, but with appreciable O(2p) character owing to hybridization with the O ligands. The Y and Ba sites are essentially magnetically inert.
27. The NMR shift K is defined by the relation $\omega_{\text{res}} = \gamma H_0(1 + K)$, where ω_{res} is the resonance frequency, γ is the gyromagnetic ratio, and H_0 is the applied field.
28. R. Kubo and Y. Obata, *J. Phys. Soc. Jpn.* **11**, 547 (1956).
29. The orbital shift coefficient is given by $\alpha_{\text{orb}} = 22.41 \langle r^{-3} \rangle_{3d} (\text{emu/mol})^{-1}$, where $\langle r^{-3} \rangle_{3d}$ is in atomic units. The spin coefficients may be written $\alpha_{1,2}^{\text{orb}} = 0.358 A_{1,2} / g_V (\text{emu/mol})^{-1}$, where $A_{1,2}$ is the total hyperfine constant in kilogauss per Bohr magneton.
30. D. E. MacLaughlin, in *Solid State Physics*, D. Turnbull, Ed. (Academic Press, New York, 1976), vol. 31, pp. 1–69.
31. W. C. Lee, R. A. Klemm, D. C. Johnston, *Phys. Rev. Lett.* **63**, 1012 (1989).
32. A. Abragam and B. Bleaney, *Electron Paramagnetic Resonance of Transition Ions* (Oxford Univ. Press, Oxford, 1970).
33. See, for example, W. E. Pickett, *Rev. Mod. Phys.* **61**, 433 (1989).
34. In (25) the orbital susceptibility components are given in this notation as $\chi_{2ab}^{\text{orb}} = 0.81 N_0 (2\mu_B^2 / \Delta_1)$ and $\chi_{2c}^{\text{orb}} = 0.81 N_0 (8\mu_B^2 / \Delta_0)$, where the leading numerical factors are estimates of orbital reduction effects, N_0 is Avogadro's number, and μ_B is the Bohr magneton.
35. The g -tensor components (32) are $g_{ab} = 2 - 2\Delta_1$ and $g_c = 2 - 8\Delta_0$.
36. The local spin hyperfine tensor coefficient is $A_{cp} + A_c^{\text{so}} + D_c \langle r^{-3} \rangle_{3d}$, representing core-polarization, spin-orbit (orbital), and dipolar contributions, respectively. Systematics for 3d ions (32) give $A_{cp} \approx -128 \text{ kG}/\mu_B \pm \sim 10\%$. The spin-orbit components are determined by the orbital shifts K_{2ab}^{orb} and K_{2c}^{orb} (25), giving $A_{ab}^{\text{so}} = 20.7 \text{ kG}/\mu_B$ and $A_c^{\text{so}} = 135.7 \text{ kG}/\mu_B$ from the shift values in Table 1. The dipolar coefficients are $D_{ab} = 17.7$ and $D_c = -35.5$, both in $(\text{au})^3 \text{ kG}/\mu_B$.
37. R. E. Walstedt *et al.*, *Phys. Rev. B* **38**, 9299 (1988); C. H. Pennington *et al.*, *ibid.* **39**, 2902 (1989); R. E. Walstedt, W. W. Warren, Jr., R. F. Bell, G. P. Espinosa, *ibid.* **40**, 2572 (1989).
38. In this analysis we follow Mila and Rice (25) in assuming $\chi_{1v}^{\text{orb}} = \chi_{2v}^{\text{orb}}$. We also adopt the estimate $\chi_{\text{dia}} = -175 \times 10^{-6} (\text{emu/mol})$ given by A. Junod *et al.*, *Physica C* **152**, 50 (1988).
39. V. Jaccarino and Y. Yafet, *Phys. Rev. A* **133**, 1630 (1964); R. E. Walstedt, J. H. Wernick, V. Jaccarino, *Phys. Rev.* **162**, 301 (1967).
40. A. K. McMahon, R. M. Martin, S. Satpathy, *Phys. Rev. B* **38**, 6650 (1988).
41. D. L. Randles, *Proc. R. Soc. London Ser. A* **331**, 85 (1972).
42. Y. Obata, *J. Phys. Soc. Jpn.* **18**, 1020 (1963).
43. P. W. Anderson and Y. Ren, in *High Temperature Superconductivity*, K. Bedell, D. Coffey, D. E. Meltzer, D. Pines, J. R. Schrieffer, Eds. (Addison-Wesley, New York, 1990), pp. 3–34.
44. See, for example, A. Narath, in *Hyperfine Interactions*, A. J. Freeman and R. B. Frankel, Eds. (Academic Press, New York, 1967), p. 287.
45. B. S. Shastry, *Phys. Rev. Lett.* **63**, 1288 (1989).
46. J. Koringa, *Physica* **16**, 601 (1950).
47. B. G. Silbernagel, V. Jaccarino, P. Pincus, J. H. Wernick, *Phys. Rev. Lett.* **20**, 1091 (1968).
48. P. C. Hammel *et al.*, *ibid.* **63**, 1992 (1989).
49. F. Mila and T. M. Rice, *Phys. Rev. B* **40**, 11382 (1989).
50. N. Bulut, D. Hone, D. Scalapino, J. E. Bickers, *ibid.* **41**, 1797 (1990).
51. A. Millis, H. Monien, D. Pines, unpublished data.
52. C. M. Varma, P. B. Littlewood, S. Schmitt-Rink, E. Abrahams, A. E. Ruckenstein, *Phys. Rev. Lett.* **63**, 1996 (1989).
53. L. C. Hebel and C. P. Slichter, *Phys. Rev.* **113**, 1504 (1959).
54. Y. Kuroda and C. M. Varma, unpublished data.
55. L. Coffey, *Phys. Rev. Lett.* **64**, 1071 (1990).
56. T. Imai *et al.*, *J. Phys. Soc. Jpn.* **57**, 1771 (1988).
57. J. M. Tranquada *et al.*, *Phys. Rev. B* **38**, 8893 (1988).
58. W. W. Warren, Jr., *et al.*, *ibid.* **39**, 831 (1989); M. Horvatic *et al.*, *ibid.*, p. 7332.
59. W. W. Warren, Jr., *et al.*, *Phys. Rev. Lett.* **62**, 1193 (1989); W. W. Warren, Jr., *et al.*, *Physica C* **162–164**, 179 (1989).
60. R. E. Walstedt *et al.*, *Phys. Rev. B* **41**, 9574 (1990).
61. M. Takigawa *et al.*, unpublished data.
62. J. Friedel, *J. Phys. Condens. Matter* **1**, 7757 (1989).
63. A. Kampf and J. R. Schrieffer, *Bull. Am. Phys. Soc.* **35**, 717 (1990).
64. This ratio is a measure of the enhancement of relaxation by correlation effects among the fermions. We modify it here by dividing by N_s , the number of fluctuation sources, assumed independent, at a given site [$N_s = 4, 2$, and 8 for Cu(2), O(2,3), and Y, respectively]. In the absence of electron-electron interactions the Korringa ratio $\rightarrow 1$.
65. We thank P. Littlewood, L. F. Mattheiss, A. Millis, M. Schluter, B. S. Shastry, and C. M. Varma for numerous helpful discussions. We are especially appreciative of M. Takigawa's willingness to allow presentation of unpublished O(2,3) NMR data on O-deficient material.



In a display of perverse brilliance, Carl the repairman mistakes a room humidifier for a mid-range computer but manages to tie it into the network anyway.